JOURNAL OF MATERIALS SCIENCE **39** (2004) 3705–3716

Topological organization and textural changes of carbon macro-networks submitted to activation with N_2 and CO_2

J. MATOS*, M. LABADY, A. ALBORNOZ, J. LAINE, J. L. BRITO
Laboratorio de Fisicoquímica de Superficies, Centro de Química, Instituto Venezolano de Investigaciones Científicas (I.V.I.C.), Apartado 21827, Caracas 1020-A, Venezuela
E-mail: jmatos@ivic.ve

Polygonal macro-networks of carbon in the form of films were synthesized by the controlled pyrolysis of saccharose with or without potassium in the form of KOH. The topological organization of these random two-dimensional networks differ significantly from other two-dimensional cellular structures. The pentagon was the most abundant polygon in the film networks, which had ring areas in the range of 4 to 12 mm^2. In addition to two-dimensional films, we also obtained irregular three-dimensional sponge-like balls featuring a random network structure similar to that obtained in the films. These sponges developed in the form of coiled tubes. We attribute the formation of these carbon macro-coils to the presence of potassium particles inside the original carbonaceous matrix. A study of textural changes of the macro-networks of carbon by activation under flow of N_2 and CO_2 has shown that activated carbon with surface areas as high as 980 $m^2 \cdot g^{-1}$ can be obtained from non-activated macro-networks. From our study of textural changes, we propose a detailed mechanism that explains the role of KOH as a catalysts for the activation of the macro-networks of carbon.

1. Introduction

Networks of cells having randomly distributed areas and numbers of sides constitute a large class of natural materials including polycrystalline structures observed in metals, ceramics, polymers, Langmuir monolayers, magnetic froths, flame cells, biological tissues, soap froths, etc. [1–10]. On the other hand, well defined, molecular networks such as fullerenes and nanotubes have been some of the most remarkable recent discoveries in the area of carbon research [11–17]. Another ill-defined type of carbon network, corresponds to the microporous structure of activated carbons (a material with many applications [18]), assumed to consist of polyhexagonal sheets of carbon, forming micropores and mesopores of widths between 10 and 500 Å [19, 20]. In addition, electron microscopy has revealed other networks in activated carbons [21]. In this case, the macropore (>500 Å width) structure observed originates from the preservation after carbonization of the biological tissue skeleton of the raw material (wood, coconut shell, etc.). Thus, at least three carbonaceous network structures form at different length scales: the molecular (fullerenes, nanotubes), the micro (microporous carbon), and the macro (macroporous carbon). Despite extensive investigation [11–27] of synthetic routes to form both molecular-network and micro-network carbon materials, few studies discuss the synthesis and characterization of macro-networks [28]. The study of the topological and textural characteristics of carbon films is of considerable interest since they relate closely both to the physical and chemical properties of these materials [29].

We can consider carbon films to be two-dimensional (2D) random cellular networks, which we treat as random partitions of the plane into cells (two-dimensional (2D) polygons with three or more sides) [1, 2, 5, 30]. The topology of natural and simulated cellular networks constrains the possible configuration of the cells, since an infinite space-filling two-dimensional network with trigonal vertices obeys the Euler topological relation [1, 2, 31–33]:

$$\langle n \rangle = \sum_n [n\rho(n)] = 6, \tag{1}$$

for the first moment of the cell-side distribution, where $\rho(n)$ is the probability of ocurrence of a cell with n sides, which corresponds to the trivial constraint on probabilities, given by:

$$\sum_n [\rho(n)] = 1 \tag{2}$$

*Author to whom all correspondence should be addressed.

References [3, 5–7, 34, 35] present detailed descriptions of some of the concepts involved in the topological definition of such random cellular structures.

This communication presents, first, the method of synthesis and the resulting topological organization of two carbonaceous macro-network 2D-films obtained by a step-wise heat treatment of saccharose with or without potassium hydroxide. Second, we study experimentally the texture changes of these carbonaceous network materials when activated at up to 800°C with N_2 or CO_2, to elucidate the potential applications of these carbonaceous materials. Our study addreses the production of network films of activated carbon that could serve as fixed co-adsorbents in heterogeneous photocatalytic processes such as the photomineralization reactions of organic pollutants in waste water [36].

2. Experimental

2.1. Network processing

We placed a solution of either 1 mL of water or 1 mL of aqueous solution (34 wt%) of potassium hydroxide (Merck, analytical grade) plus 2 g of D(+)-saccharose (Merck, bacteriology grade) in a 50 mL pyrex beaker and stirred it at 80°C until the solution became viscous and light brown. Immediately, we remove the heat and left the solutions until the saccharide recrystalized as an homogeneous and transparent sheet at the bottom of the beaker.

We then applied two consecutive heat treatments to the sheets: first, a low temperature stabilization treatment inside an oven (static air) at the following temperatures: 60, 90, 110, and 130°C, for 10 min at each temperature using heating rates between steps of about $3°C \cdot min^{-1}$. This initial heat treatment aims to promote very slow and homogeneous expansion of the saccharide film along the beaker walls up to its exterior border, since the final stabilization temperature corresponds to the beginning of the glass transition of saccharose. The second heat treatment consists of carbonization under an inert flow of nitrogen ($\cong$100 mL $\cdot$ min^{-1}) using the following step temperatures: 50, 100, 150, 200, 250, 350°C, soaking 30 min at each temperature, and finally 1 h at 450°C, using heating rates between steps of about $5°C \cdot min^{-1}$. The final 450°C carbonization temperature is optimal for the production of low-temperature (L-type) activated carbon from lignocellulosic raw materials [37, 38].

We denote these carbonaceous macro-network samples as $A_{NW\text{-}1}$ and $A_{NW\text{-}2}$, for the saccharose dissolved in water or in the KOH solution, respectively.

2.2. Statistical characterization of macro-network films

Our statistical analysis of photographs of the macro-network films $A_{NW\text{-}1}$ and $A_{NW\text{-}2}$ (three samples for each set of conditions) is followed as in previous studies of other cellular structures [1, 2, 5]. We analysed a total of 750 and 558 cells, respectively, for the $A_{NW\text{-}1}$ and $A_{NW\text{-}2}$ samples, and the error in measuring cell areas was less than 5%. We found polygonal cells with from three to nine sides. We measured the probability of ocurrence of cells with n sides $\rho(n)$, the distribution of areas of n-sided cells, $\rho(A_n)$, and the average polygon areas for each topology $\langle A_n \rangle$ by an analytical method that we have previously employed [28]. We obtained the average polygonal areas $\langle A_n \rangle$ as the product of the distribution of areas of n-sided cells $\rho(A_n)$ with the actual geometric size of each of the photographed samples according to the magnification factor of the photographies.

2.3. Activation processing of the networks

Besides the macro-network films we also obtained two types of carbonaceous three-dimensional (3D) networks, that we used to study textural changes during activation processing. We performed the activations in a tubular furnace, under either inert N_2 flow ($\cong$100 mL $\cdot$ min^{-1}) with several final residence times: 5, 60, 120 and 300 min at constant final temperature of activation equal to 800°C; or under CO_2 flow ($\cong$100 mL $\cdot$ min^{-1}) at the following temperatures of activation: 700, 750 and 800°C, with a constant residence time of 5 min.

2.4. Textural characterization of the networks

We used N_2 adsorption at 77°K to characterize the texture of the macro-networks ($A_{NW\text{-}1}$ and $A_{NW\text{-}2}$) and the activated network materials in terms of the B.E.T. surface areas. We measured the full isotherms in the range of 0.03 to 630 Torr using an ASAP-2010 apparatus from Micromeritics. For experimental details see [39, 40].

3. Results and discussion

3.1. Statistical analysis of macro-network films

A previous communication [28] described the topological organization of the $A_{NW\text{-}1}$ macro-networks. The present work describes the topological organization of both macro-networks films $A_{NW\text{-}1}$ and $A_{NW\text{-}2}$, but shows photographs only for the $A_{NW\text{-}2}$ samples.

In both samples, two- and three-dimensional macro-networks were formed simultaneously during carbonization. The macro-network films adhered both to the bottom and the cylindrical beaker walls, covering approximately one third and one half of the beaker height, respectively, for the $A_{NW\text{-}1}$ and $A_{NW\text{-}2}$ samples. Fig. 1a shows a typical $A_{NW\text{-}2}$ macro-network, consisting of a random net of polygonal ring cells, each formed by grains of carbonaceous material. Both $A_{NW\text{-}1}$ (not shown) and $A_{NW\text{-}2}$ (Fig. 1a) had polygons from three up to eight or nine sides. After thermal treatment, the $A_{NW\text{-}2}$ sample has carbonaceous material between the cells while the $A_{NW\text{-}1}$ film sample does not. The inside of the $A_{NW\text{-}2}$ network cells is not empty as in the $A_{NW\text{-}1}$ films. Fig. 1b shows a particular $A_{NW\text{-}2}$ sample that has "T" type vertices with an internal angle $\theta = 180°$. In several types of random network, particularly solidified polymer films with topological organization

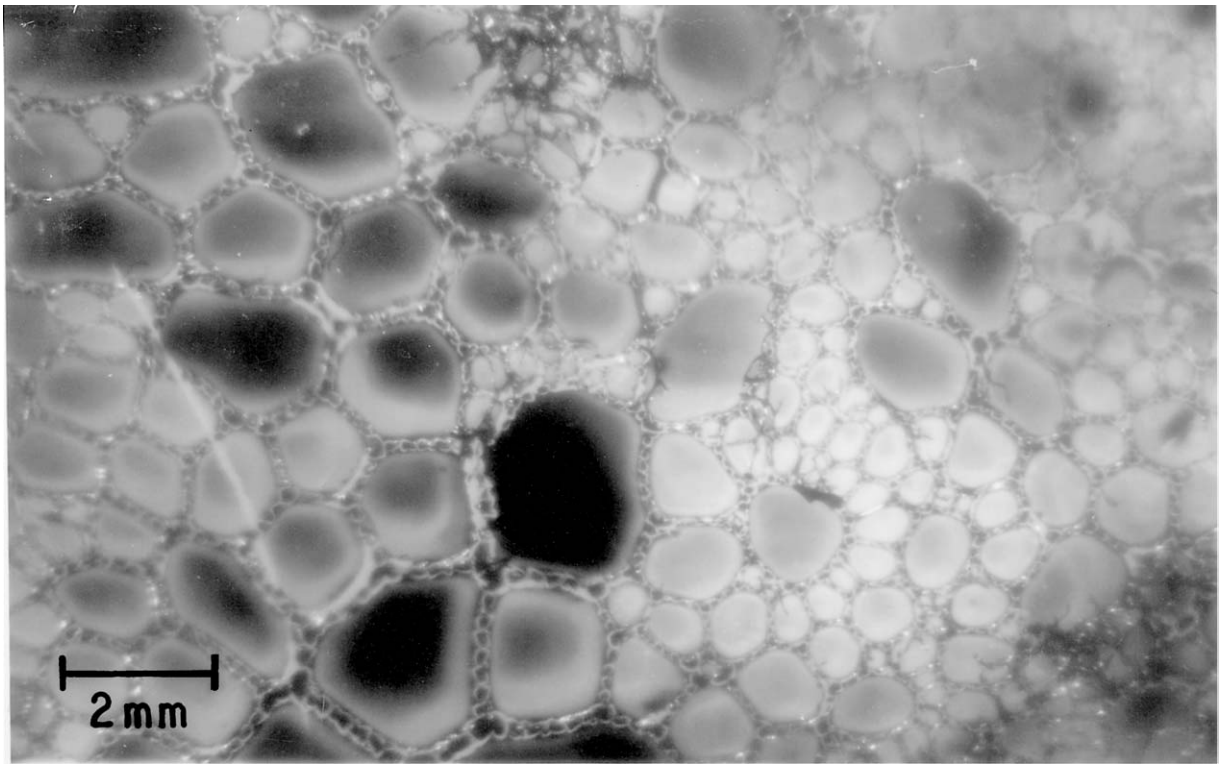

(a)

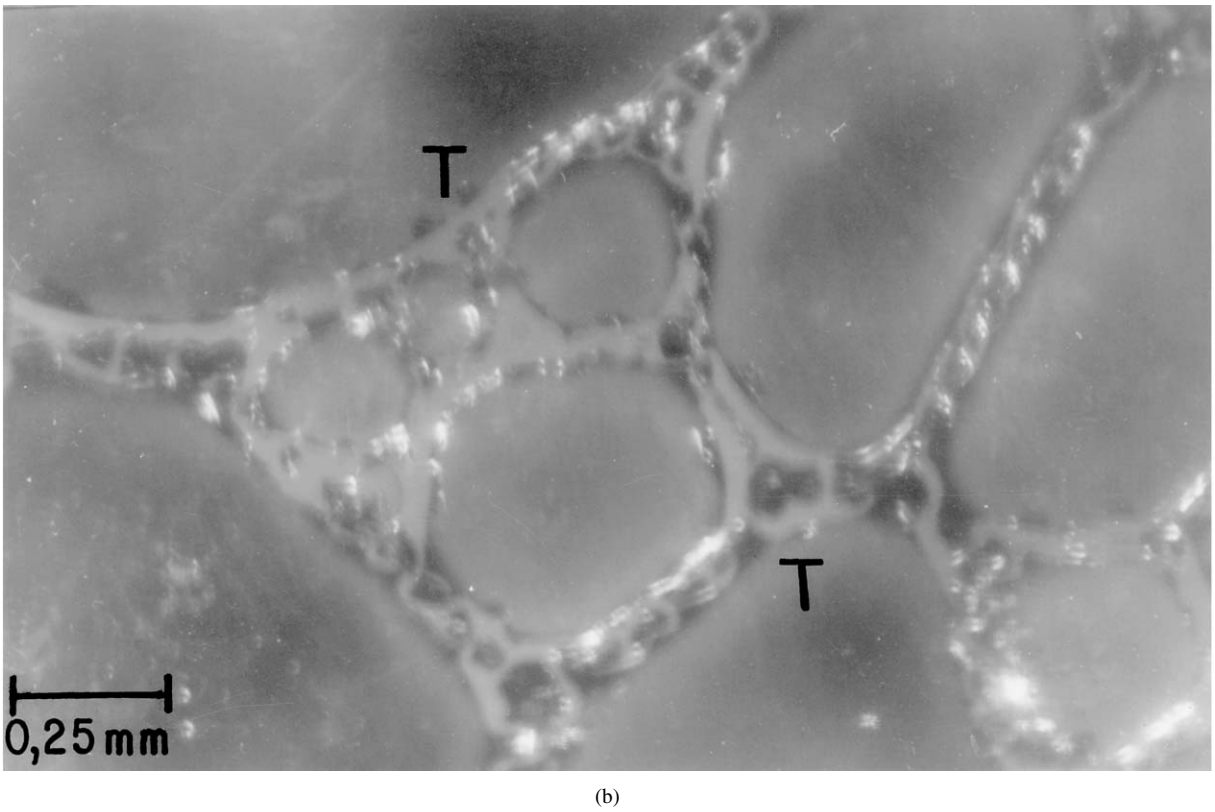

(b)

Figure 1 Images of the carbonaceous macro-network film from the $A_{\text{NW-2}}$ sample adhering to the pyrex beaker: (a) Typical random pattern showing the predominance of five-sided cells and (b) A subsection showing the presence of "T" type vertices with internal angle $\theta = 180^{\circ}$.

very similar to the present macro-networks, the T-type vertices results from the dynamics of cell formation [1, 2].

Fig. 2 shows the abundance of n-sided polygons $\rho(n)$ obtained from the statistical analysis of 750 and 558 cells, respectively, for $A_{\text{NW-1}}$ and $A_{\text{NW-2}}$ macro-network films. Both distributions are similar with pentagons most abundant and:

$$\langle n \rangle_{\text{ANW-1}} = 5.155 \tag{3}$$

$$\langle n \rangle_{\text{ANW-2}} = 5.161 \tag{4}$$

Although the low value of $\langle n \rangle$ occurs in microscopic solidified polymer films [1, 2], most macroscopic

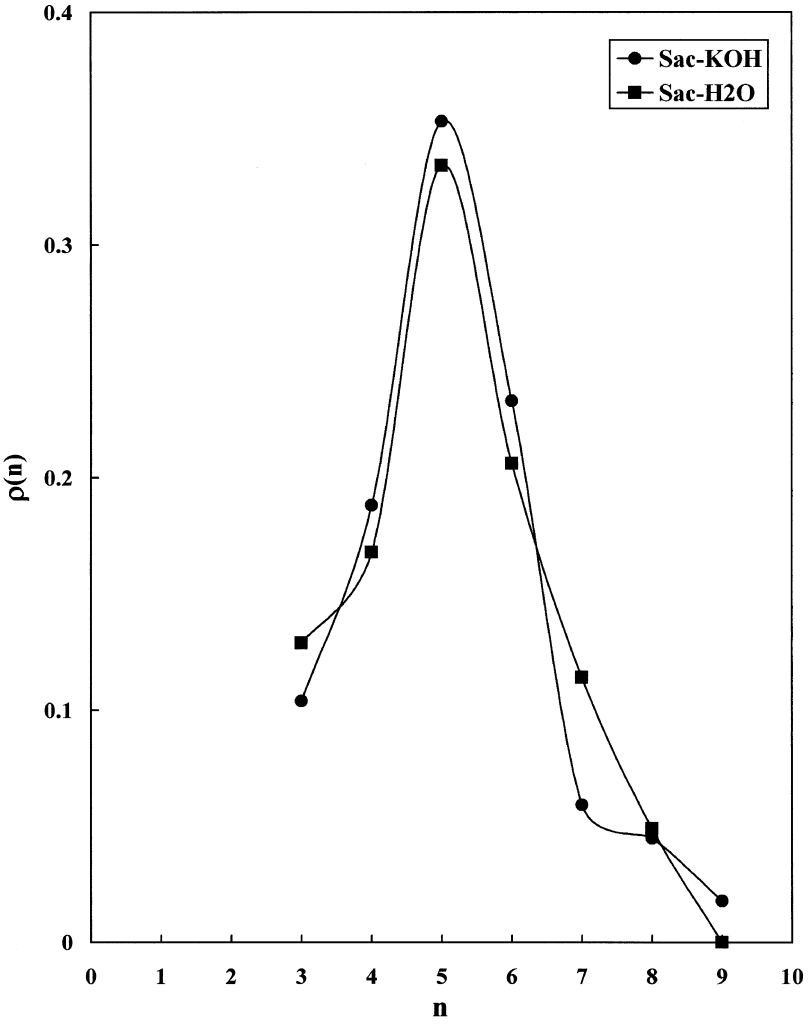

Figure 2 Polygonal distributions of the macro-networks from the $A_{NW\text{-}1}$ (Sac-H_2O) and $A_{NW\text{-}2}$ (Sac-KOH) films.

cellular structures have hexagon as the most abundant polygon as shown in Table I.

Fig. 3 shows the fraction of the total area in n-sided cells $\rho(A_n)$ of both macro-networks. The distributions are practically identical and at $n = 5$, $\rho(A_5) > \rho(A_6)$. Again, these results agree with microscopic polymer films noted above [1, 2], and differ from those in other micro- and macroscopic random networks, such as polycrystalline SCN [3–6], polycrystalline metals [4, 5], soap froths [7], flame cells [8], Langmuir monolayer [9], and magnetic froths [10]. Therefore, two-dimensional carbon macro-networks geometric properties differ intrinsically from those in other types of network.

TABLE I Comparison of peak values in cell-side distributions $\rho(n)$ for various materials

System	Peak n-value	$\rho_{(5)}$	$\rho_{(6)}$	Reference
$A_{NW\text{-}1}$	5	0.334	0.206	Present work
$A_{NW\text{-}2}$	5	0.353	0.233	Present work
Polymer polygrain	5	0.392	0.25	[1]
Flame cells	5.4	0.36	0.34	[8]
Soap froths	5.5	0.3	0.3	[7]
Langmuir monolayer	6	0.225	0.345	[9]
Polycrystalline metal	6	0.267	0.4	[4]
Polycrystalline SCN	6	–	–	[3, 6]
Magnet froth	6	0.25	0.55	[10]

Fig. 4 shows that for both macro-networks, the average cell areas of an n-sided cell, $\langle A_n \rangle$, is linear in n (with correlation coefficients close to 1 in both cases):

$$\langle A_n \rangle = (0.007\ \text{mm}^2) + (1.235\ \text{mm}^2)n \quad (5)$$

$$\langle A_n \rangle = (-0.0011\ \text{mm}^2) + (1.2988\ \text{mm}^2)n \quad (6)$$

for $A_{NW\text{-}1}$ and $A_{NW\text{-}2}$, respectively. Although this linear behaviour is consistent with Lewis Law [1, 2, 41], the constants in Equations 5 and 6, differ from those reported for other types of random network [1–10]. Table II shows that most cell areas fall inside the range 4 to 10 mm^2 and 4 to 12 mm^2, for $A_{NW\text{-}1}$ and $A_{NW\text{-}2}$, respectively. Therefore, the average values, $\langle a \rangle$, for each case are: 6.7993 and 7.7921 mm^2, indicating that the Lewis constants (λ) for the present work are: 0.1816 and 0.1667, which are similar to the values reported ($\lambda = 1/4$) [1, 2, 41].

3.2. Morphological characteristics and chemical composition of the carbonaceous macro-networks

In addition to two-dimensional films, irregular sponge-like balls form in the bottom of the beakers. Fig. 5 shows an image of a part of the carbonaceous bulk in an $A_{NW\text{-}2}$

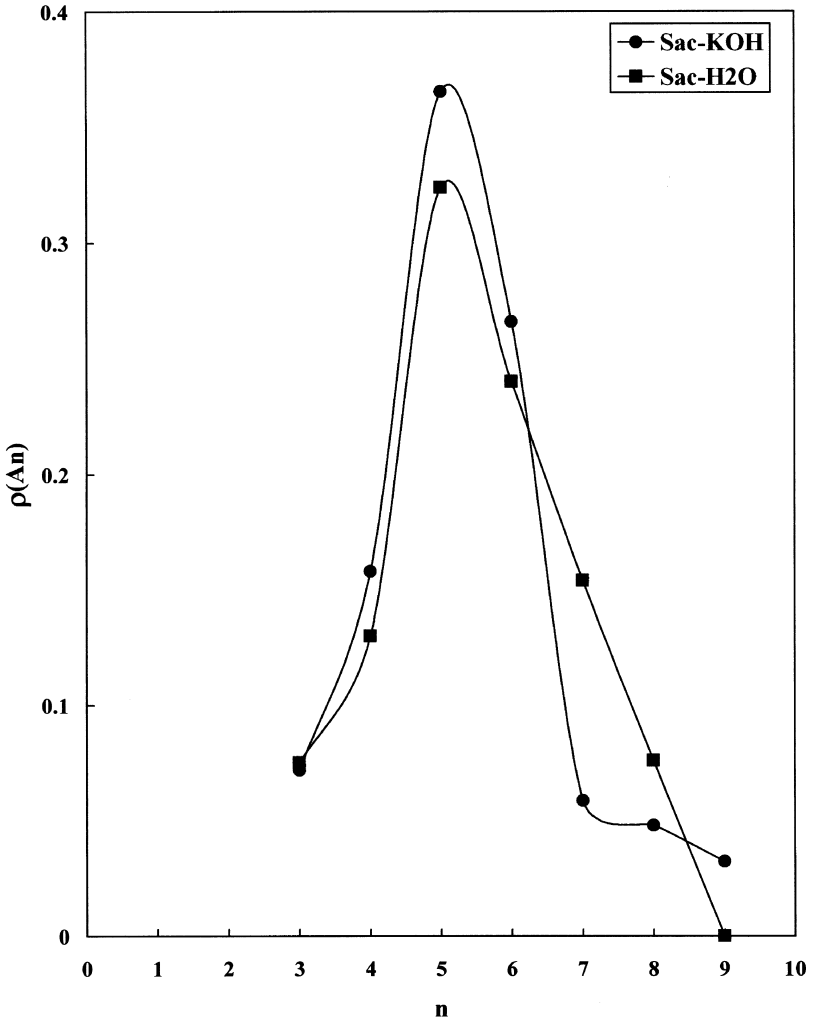

Figure 3 Distributions of areas in the macro-networks from the $A_{NW\text{-}1}$ (Sac-H_2O) and $A_{NW\text{-}2}$ (Sac-KOH) films.

sample. Fig. 5a shows that this three-dimensional feature resembles the 2D random network in the same material (Fig. 1), a random network of polygonal carbonaceous grains of different sizes. For both types of sample, the sponges connect loosely to the film network. Moreover, the noticeable separation of the polygons (Figs 1 and 5) suggest weak linking, which most probably leads to the easy disconnection of the sponge balls from the films adhered to the beaker's wall.

The carbonaceous grain structure observed in Fig. 5b does not satisfy Lewis' Law [2, 41], suggesting that the nucleation time for the different grains in the matrix is not the same. This is explained as follows: By comparing several images of the two- and the three-dimensional $A_{NW\text{-}2}$ macro-networks, we found several interfaces where the carbon grains developed into a continuous 3D polygonal net of macrotubes (Fig. 5b). Perhaps the carbonaceous macro-networks, form in a way similar to those of carbon nanotubes [42].

Fig. 5b shows a surprising morphology. Some of the cells have coiled shapes [26, 43, 44] (denoted mcs in Fig. 5b). Several authors have described the formation of coiled carbon tubes and their growth mechanism [26, 43, 44]. Carbon tube nano-coils form due to the presence of iron or indium and tin oxide films acting as catalysts, mainly in thermal chemical vapor deposition. Certain metal species tend to migrate through carbonaceous deposits formed during catalytic vapor-chemical decomposition of hydrocarbons to produce carbon nano-tubes, filaments and vapor-growth fibers [45]. We attribute our carbon macro-coils to the presence of potassium microparticles in the carbonaceous matrix, indirectely confirmed by the absence of macro-coiled carbon filaments in the $A_{NW\text{-}1}$ sponge which lacks potassium [28]. In macroscopic morphology the $A_{NW\text{-}1}$ sponge [28] resembles typical reticulated glassy carbon foams with a pentagonal dodecahedron structure as those obtained in polystyrene and polyurethane

TABLE II Average areas of n-sided cells, $\langle A_n \rangle$, of the $A_{NW\text{-}1}$ and $A_{NW\text{-}2}$ macro-network films as a function of n

n sided-cells	$n = 3$	$n = 4$	$n = 5$	$n = 6$	$n = 7$	$n = 8$	$n = 9$
$[\langle A_n \rangle]$ for $A_{NW\text{-}1}$ (mm^2)	3,708	4,948	6,186	7,416	8,656	9,882	–[a]
$[\langle A_n \rangle]$ for $A_{NW\text{-}2}$ (mm^2)	3,896	5,194	6,493	7,792	9,090	10,39	11,69

[a]Polygonal cells of 9-sides were not present in the $A_{NW\text{-}1}$ sample.

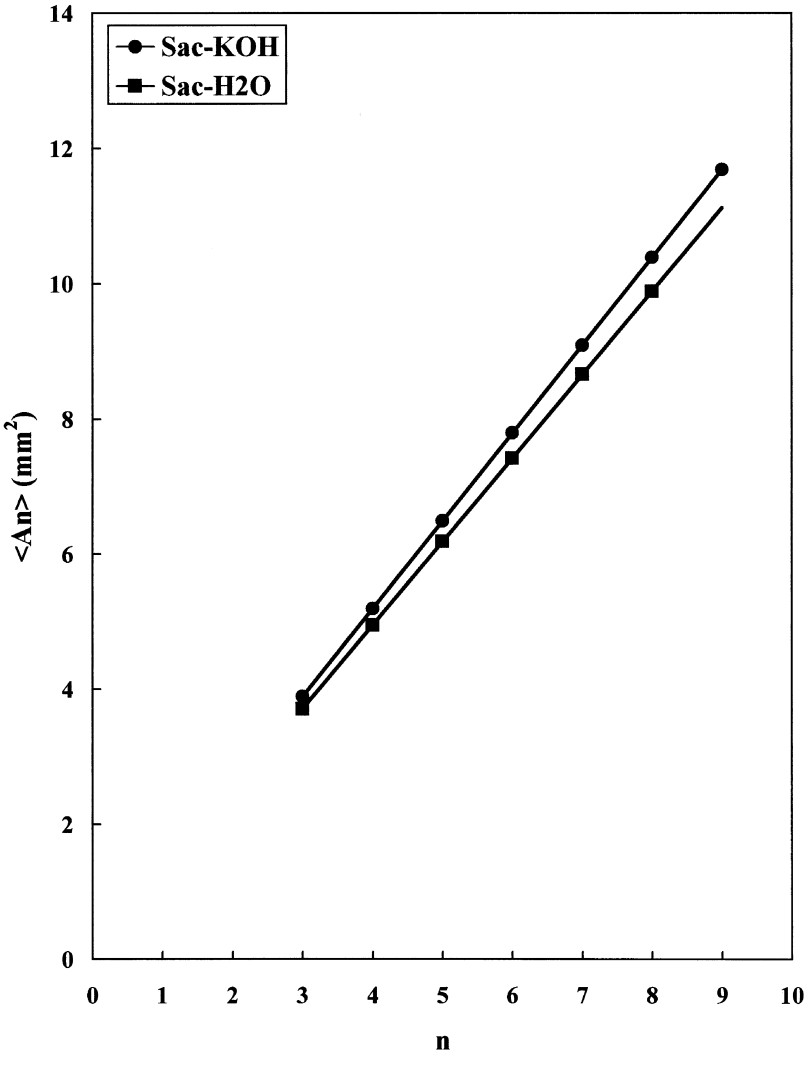

Figure 4 Average polygonal areas in the macro-networks from the A_{NW-1} (Sac-H_2O) and A_{NW-2} (Sac-KOH) films.

foam insulations [46] or from thermal processing of mesophase pitches [47].

Compairing Figs 1 and 5, shows that 3D cells have void spaces between cells indicating that the bulk of the material was consumed by pyrolysis because the adhesion forces to the pyrex wall reduced volatilization in the 2D films.

During carbonization the material volume increases remarkably, particularly, in the saccharose sample dissolved in KOH solution (A_{NW-2}). Table III shows that the large increase in volume during carbonization in the 3D A_{NW-2} sample results in a lower density than for the A_{NW-1} sample (0.0156 g/cm^3 against 0.0223 g/cm^3). We estimated the apparent densities in Table III from the ratio between the weights of different masses of the samples (mechanically compressed into a graduated cylinder) and their volume after substracting the theorical remnant weight of potassium (as K_2O) in the A_{NW-2} sample. As we described above, for 1 mL 34 wt% of aqueous KOH solution, the weight of K_2O is 0.4501 g.

TABLE III Apparent density, ρ_{app}, of the 3D A_{NW-1} and A_{NW-2} macro-network materials

Network	ρ_{app} (g/cm^3)
A_{NW-1}	0.0223 ± 0.0009
A_{NW-2}	0.0156 ± 0.0006

Since our carbonaceous materials are a complex biphasic arrangement of crystalline lamellar and amorphous phases, we expect topological effects at boundaries between crystalline-crystalline and crystalline-amorphous phases [2]. Since the present networks are saccharose-based carbons, we expect textural changes during thermal activation at temperatures higher than those employed for the carbonization [27, 48].

Several results of Laine and co-workers [28, 38, 49] reinforce the above suggestion. Thus, elemental analysis of the "blank" macro-network (A_{NW-1}) has shown [28] a chemical composition of: C = 61%, O = 36%, and H = 3% (wt%), which corresponds to $C_8H_4O_4$. Compared to the saccharose base $C_{12}H_{22}O_{11}$ the hydrogen and oxygen decrease by 4 and 12 wt% respectively, and the carbon increases by 16 wt%. On the other hand, nitrogen adsorption in the A_{NW-1} and A_{NW-2} macro-networks was undetectable, indicating negligible B.E.T (Brunauer-Emmett-Teller) surface areas [28], unlike activated carbon which normally has around 1000 m^2/g surface area [18]. As will be seen below, the present 3D macro-networks have relatively large cells which are more than 100 times wider than the macropores found in carbons derived from lignocellulosic raw

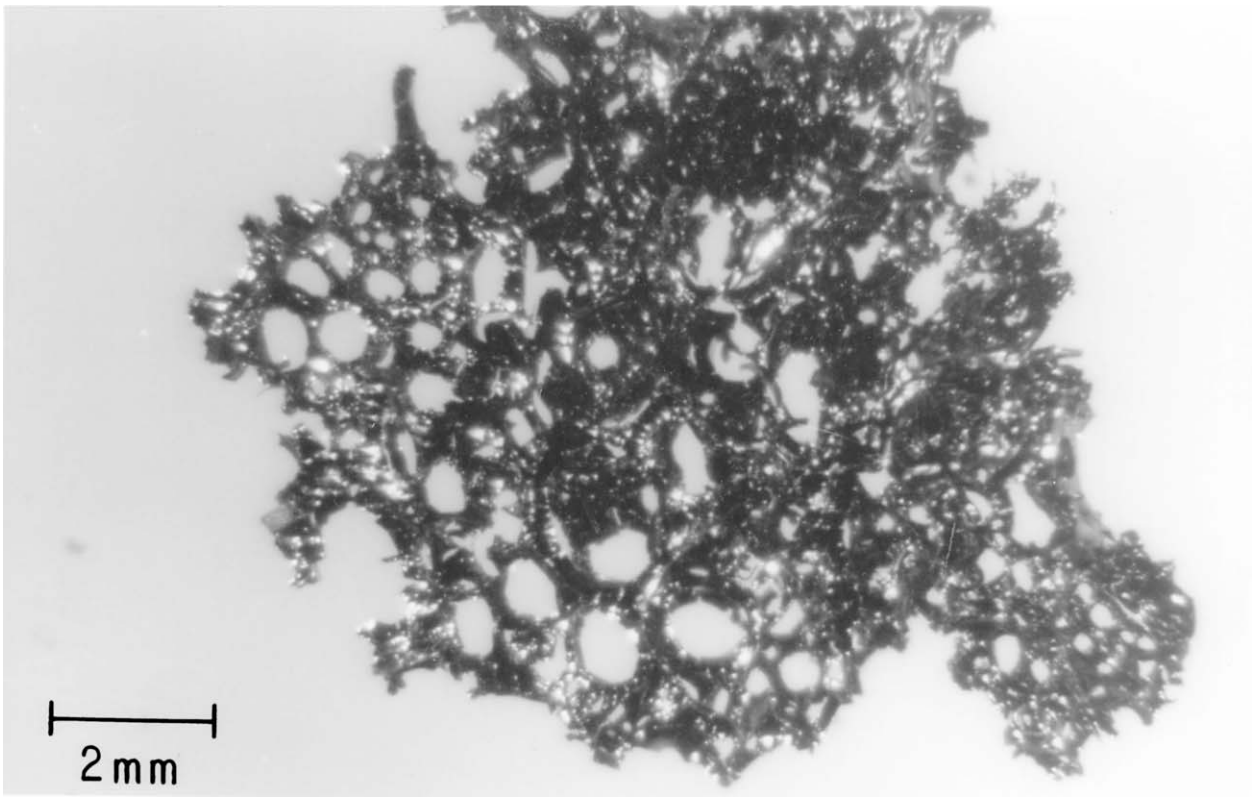

(a)

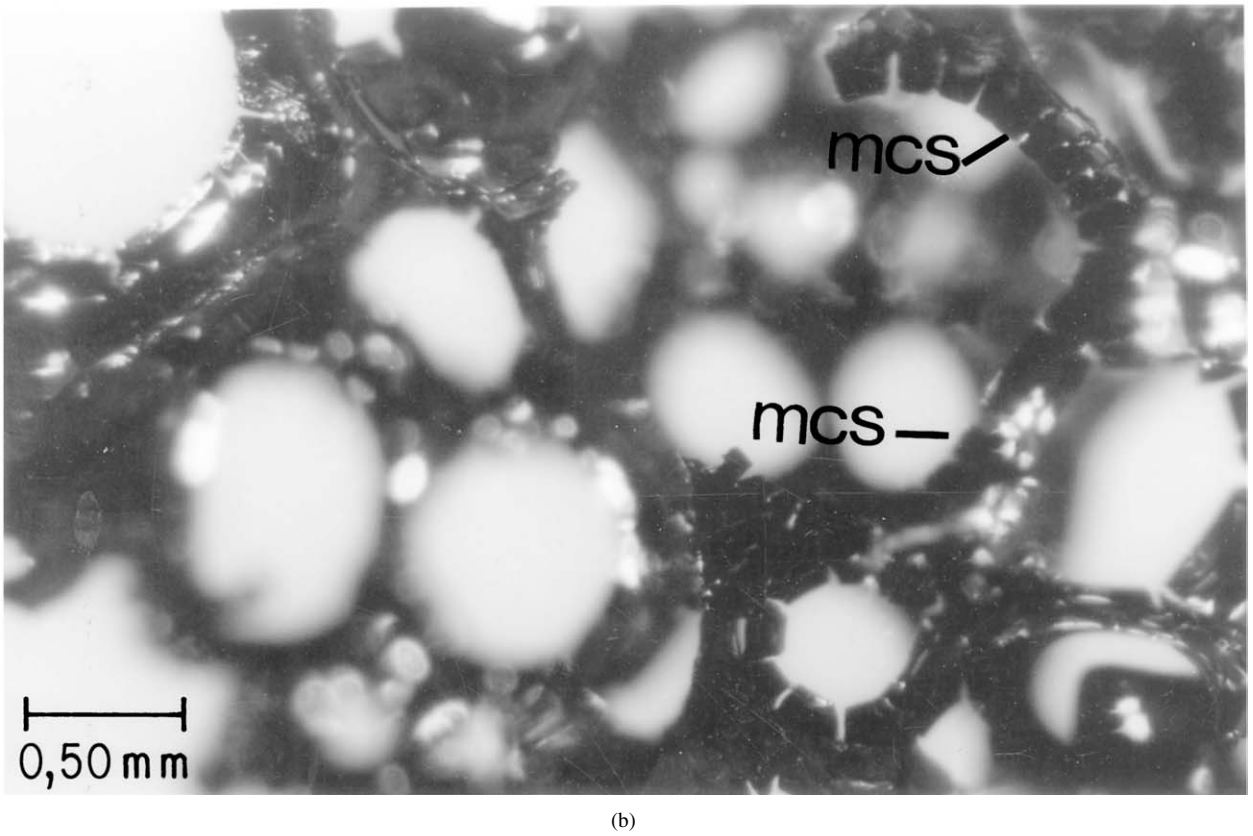

(b)

Figure 5 Image of bulk carbonaceous macro-network from the A_{NW-2} sample: (a) 3D random structure of a subsection of the sponge and (b) Subsection showing macrocoil shapes (mcs).

materials (agreeing with the B.E.T. surface areas for A_{NW-1} and A_{NW-2} samples listed in Table V). Finally, a temperature programmed reduction (TPR) analysis of the network blank material [28, 49] has shown a TPR trace resembling those reported [38] for L-type activated carbons; i.e., those prepared by low temperature-"chemical"-activation, a synthesis method that uses a chemical additive (normally H_3PO_4, $ZnCl_2$, KOH, etc.). In that work, after a first positive peak in the TPR spectrum attributed to H_2-reduction of the carbonaceous material (consumption of hydrogen), a high temperature negative peak (which is not observed in

TABLE IV Summary of the experimental conditions employed for the study of texture changes of the 3D macro-networks under activation by N_2 and CO_2

Networks	Activation temperature (°C)	Activation residence time(min)	Other experimental conditions
$A_{N_2\text{-}2}$	800	60	N_2-activated from $A_{NW\text{-}1}$, without H_2O pre-washing
$A_{CO_2\text{-}2}$	800	60	CO_2-activated from $A_{NW\text{-}1}$, without H_2O pre-washing
$A_{N_2\text{-}3}$	800	60	N_2-activated from $A_{NW\text{-}2}$, with H_2O pre-washing
$A_{CO_2\text{-}3}$	800	60	CO_2-activated from $A_{NW\text{-}2}$, with H_2O pre-washing
$A_{N_2\text{-}4A}$	800	60	N_2-activated from $A_{NW\text{-}2}$, without H_2O pre-washing
$A_{N_2\text{-}4B}$	800	120	N_2-activated from $A_{NW\text{-}2}$, without H_2O pre-washing
$A_{N_2\text{-}4C}$	800	300	N_2-activated from $A_{NW\text{-}2}$, without H_2O pre-washing
$A_{N_2\text{-}4D}$	800	5	N_2-activated from $A_{NW\text{-}2}$, without H_2O pre-washing
$A_{CO_2\text{-}4A}$	800	60	CO_2-activated from $A_{NW\text{-}2}$, without H_2O pre-washing
$A_{CO_2\text{-}4B}$	800	5	CO_2-activated from $A_{NW\text{-}2}$, without H_2O pre-washing
$A_{CO_2\text{-}4C}$	750	5	CO_2-activated from $A_{NW\text{-}2}$, without H_2O pre-washing
$A_{CO_2\text{-}4D}$	700	5	CO_2-activated from $A_{NW\text{-}2}$, without H_2O pre-washing

H-type activated carbons; i.e., those prepared by high temperature-"physical"-activation) was assigned to hydrogen evolution from the macro-network material [28, 49].

The earlier results indicate activating the $A_{NW\text{-}1}$ and $A_{NW\text{-}2}$ samples is possible to obtain activated carbons showing large B.E.T. surface areas but also that they might be usable for hydrogen storage [45].

3.3. Textural changes in the networks caused by activation

3.3.1. General discussion

To confirm that high temperature heat treatments change the topology and texture of carbon macro-networks we studied activation with N_2 and CO_2 of both 3D networks. Table IV summarizes the samples and experimental conditions.

The first section of Table IV, includes two samples of $A_{NW\text{-}1}$ activated under N_2 ($A_{N_2\text{-}2}$) or CO_2 ($A_{CO_2\text{-}2}$) at 800°C for 1 h. Since $A_{NW\text{-}1}$ has no potassium the blank was not washed with H_2O before activation.

The second section of Table IV includes two samples with potassium ($A_{NW\text{-}2}$) activated under N_2 ($A_{N_2\text{-}3}$) or CO_2 ($A_{CO_2\text{-}3}$) at 800°C for 1 h. Before activating $A_{NW\text{-}2}$ we washed it with H_2O until it reached a neutral pH. To compare the $A_{N_2\text{-}3}$ and $A_{CO_2\text{-}3}$ samples with the $A_{N_2\text{-}2}$ and $A_{CO_2\text{-}2}$ samples, we substract the potassium originally in the $A_{NW\text{-}2}$ carbonaceous matrix.

The third section includes four samples with potassium ($A_{NW\text{-}2}$) activated under N_2 at 800°C for different activation times (5, 60, 120, and 300 min). We designate these samples $A_{N_2\text{-}4i}$. To study the influence of the potassium in activation, we did not wash the $A_{NW\text{-}2}$ with H_2O before activation.

Finally, the last section of Table IV shows four samples with potassium ($A_{NW\text{-}2}$) activated under CO_2 at activation temperatures from 700 up to 800°C and with activation residence times from 5 to 60 min. We designate these samples as $A_{CO_2\text{-}4i}$. As in the previous Section, to study the influence of potassium on activation, we did not wash with H_2O before activation. We hope to compare the influence of both the choice of gas and of potassium on total burn-off of saccharose and the B.E.T. surface in the two types of activation.

TABLE V Total burn-off of saccharose and B.E.T. surface areas of the 3D networks

Networks	Saccharose burn-off [a] (%)	B.E.T. surface area ($m^2 \cdot g^{-1}$)
$A_{NW\text{-}1}$	85	10
$A_{NW\text{-}2}$	66	15
$A_{N_2\text{-}2}$	92	8
$A_{CO_2\text{-}2}$	91	270
$A_{N_2\text{-}3}$	70	79
$A_{CO_2\text{-}3}$	72	137
$A_{N_2\text{-}4A}$	72	558
$A_{CO_2\text{-}4A}$	100	–[b]

[a]Except for the values for $A_{N_2\text{-}3}$ and $A_{CO_2\text{-}3}$ which were washed with H_2O, all the saccharose burn-off (%) values were estimated after subtracting the theoretical reminant weight of potassium as K_2O (≈0.4501 g).

[b]The B.E.T. surface area of the $A_{CO_2\text{-}4A}$ sample is not included since it was totally pyrolyzed.

The B.E.T. surface areas of the $A_{NW\text{-}1}$ and $A_{NW\text{-}2}$ samples listed in the Table V (10 and 15 $m^2 \cdot g^{-1}$) suggest a non-porous texture, in line with the morphology observed in Fig. 5, which shows that the 3D macro-networks of carbon have relatively large cells more than 100 times wider than the macropores found in carbons derived from lignocellulosic raw materials. The optimum temperature for L-type activated carbon synthesis is 450°C [37, 38], which is the same final temperature we employed to prepare our macro-network. Table V shows that the burn-off in our experiments was relatively high (about 85%) for $A_{NW\text{-}1}$ compared to normal chemical activation (40–60%). However, the burn-off (Table V) in the $A_{NW\text{-}2}$ sample (with potassium) is only slightly higher than normal (about 66%).

The total burn-off obtained in the $A_{N_2\text{-}2}$ and $A_{CO_2\text{-}2}$ samples is slightly higher (respectively, 92 and 91%) than that of $A_{NW\text{-}1}$ (85%). In addition, the total burn-off for the $A_{N_2\text{-}3}$ and $A_{CO_2\text{-}3}$ samples is slightly higher (respectively, 70 and 72%) than that of $A_{NW\text{-}2}$ (66%), only slightly higher than the normal range for chemical activation. This is in line with reports by Laine and coworkers [20, 21, 38, 39, 50] which propose that the chemical activator (H_3PO_4 and/or KOH) supresses volatilization and pyrolysis that would destroy the fine microporous

which causes the high surface area of L-type activated carbon. In high oxidation activation with CO_2 ($A_{CO_2\text{-}2}$ sample) the B.E.T. surface area obtained from $A_{NW\text{-}1}$ was moderate (270 $m^2 \cdot g^{-1}$) while it was negligible when activated with N_2 ($A_{N_2\text{-}2}$ sample). However, the B.E.T. surface areas for the $A_{N_2\text{-}3}$ and $A_{CO_2\text{-}3}$ samples show a different trend. Activation of $A_{NW\text{-}2}$ under N_2 ($A_{N_2\text{-}3}$) produced a higher B.E.T. surface area than for the $A_{N_2\text{-}2}$ sample obtained from $A_{NW\text{-}1}$ (79 against 8 $m^2 \cdot g^{-1}$). Activated under CO_2, the $A_{CO_2\text{-}3}$ sample produced a lower B.E.T. surface area than did the $A_{CO_2\text{-}2}$ sample (137 against 270 $m^2 \cdot g^{-1}$). These surface areas seem to indicate that although the $A_{NW\text{-}2}$ sample was previously washed with H_2O, it still contained a small amount of potassium, sufficient to inhibit excesive pyrolysis and hence to increase the B.E.T. surface area for activation under nitrogen compared to activation of $A_{NW\text{-}1}$ under N_2 ($79 \gg 8$ $m^2 \cdot g^{-1}$). In other words, KOH is an effective catalyst for the activation of the carbonized $A_{NW\text{-}2}$ macro-network, both in the presence of N_2 and CO_2.

KOH at the surface of the carbonized lignocellulosic material decomposes according to the reaction [50]:

$$2KOH \rightarrow K_2O + H_2O, \tag{7}$$

producing gaseous water that due to its small weight and molecular diameter diffuses easily into the carbon pores, contributing to gasification. The basic reaction of carbon with water vapor is endothermic and of the following stoichiometry [21, 51]:

$$H_2O + C \rightarrow CO + H_2, \quad \Delta H = +117 \text{ kJ} \cdot \text{mol}^{-1}. \tag{8}$$

In addition, the abundant oxygen available from the carbonaceous matrix can consume the yield products of Equation 8 ($CO + H_2$):

$$CO + H_2 + 2O \rightarrow CO_2 + H_2O, \tag{9}$$

further increasing the concentrations of activators ($CO_2 + H_2O$).

Yuhn and Wolf [52] have shown that other metal alkaline salts, like sodium nitrate and hydroxide, interact with carbon to form surface carbonate species. Accordingly, the formation of a layer of oxides (similarly to the layer of polyphosphate reported by Laine and Calafat [50]) over the developing pore structure could prevent the excessive gasification found for catalysis with potassium hydroxide, due to interaction with gaseous CO_2.

Like the gasification reaction of Equation 8, the reaction of carbon with carbon dioxide can be expressed as:

$$CO_2 + C \rightarrow 2CO, \quad \Delta H = +159 \text{ kJ} \cdot \text{mol}^{-1}. \tag{10}$$

On the other hand, above 800°C the water-gas shift reaction is at equilibrium [51]:

$$CO + H_2O \rightleftarrows CO_2 + H_2 \tag{11}$$

with an equilibrium constant between 0.5 and 1. Both reactions (8) and (10) are important. Though superheated steam is usually the primary activater, it is not in our case, so we suggest that reactions (7) to (9) predominate during activation of macro-networks with N_2, while reactions (7) to (11) and particularly reactions (10) and (11) are all involved during the activation of macro-networks with CO_2.

The last section of Table V ($A_{N_2\text{-}4A}$ and $A_{CO_2\text{-}4A}$ samples), suggest that this mechanism not only is in line (via reactions (7) to (9)) with the moderate burn-off of saccharose (72%) and relative high surface area (558 $m^2 \cdot g^{-1}$) of the $A_{NW\text{-}2}$ sample (with potassium) activated with N_2 at 800°C for 1 h ($A_{N_2\text{-}4A}$), but also, (via reactions (10) and (11)) with the maximum burn-off of saccharose (100%) observed for the $A_{NW\text{-}2}$ sample (with potassium) activated with CO_2 at 800°C for 1 h ($A_{CO_2\text{-}4A}$). In neither $A_{N_2\text{-}4A}$ and $A_{CO_2\text{-}4A}$ was the macro-network ($A_{NW\text{-}2}$) washed with water before activation so they contained all the remnant potassium. The last section of Table V suggest that the presence of potassium as KOH initiates, by means of reaction (7), the catalytic activation of the carbonaceous network. This effect is stronger for the sample activated under CO_2 ($A_{CO_2\text{-}4A}$) where the macro-network sample ($A_{NW\text{-}2}$) was totally pyrolyzed probably by the increased amounts of activators ($CO_2 + H_2O$) produced by reaction (11).

3.3.2. Influence of the activation time

Fig. 6 shows the B.E.T. surface areas and the total burn-off of saccharose estimated after substracting the theoretical remnant weight of potassium as K_2O (≈0.4501 g). $A_{NW\text{-}2}$ samples activated under N_2 at

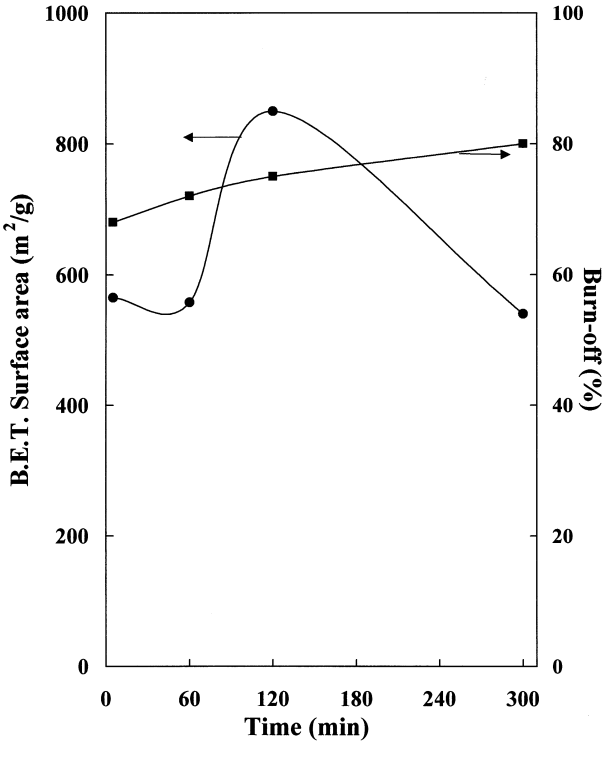

Figure 6 Surface B.E.T. areas and burn-off behaviour of networks activated with N_2 (at 800°C) as a function of residence time.

800°C as a function of the residence activation time were designated $A_{N_2\text{-}4i}$. The burn-off tends to increase with the activation time, a well-known trend reported for several types of lignocellulosic materials [53–60]. The burn-off of the $A_{N_2\text{-}4i}$ samples shown in Fig. 6 increases from 68% at 5 min to close to 80% at 300 min, principally through reactions (7) to (9). The quantities of activators ($CO_2 + H_2O$) produced by reaction (9), may increase strongly at longer activation times leading to greater activation and more pyrolysis of the saccharose. The B.E.T. surface areas for the $A_{N_2\text{-}4i}$ samples, in Fig. 6 show that the texture of the macro-network ($A_{NW\text{-}2}$) changes as a function of the residence time, the surface area increasing from 565 $m^2 \cdot g^{-1}$ at 5 min ($A_{N_2\text{-}4D}$) to a value of 558 $m^2 \cdot g^{-1}$ at 60 min (A_{N_2-4A}) to a maximum of 850 $m^2 \cdot g^{-1}$ at 120 min ($A_{N_2\text{-}4B}$); then drastically falling to 540 $m^2 \cdot g^{-1}$ at 300 min ($A_{N_2\text{-}4C}$). For activation times longer than 2 h, activation seems to became less efficient, probably due to the well-known destruction of the fine micropore structure which produces the high surface area of L-type activated carbons [20, 21, 37, 38]. The results in Fig. 6 agree with this mechanism, so reactions (7) to (9) are probably the main cause of texture changes during activation of the $A_{NW\text{-}2}$ macro-network under N_2 at 800°C.

3.3.3. Influence of the activation temperature

We now discuss the $A_{NW\text{-}2}$ macro-network samples designated $A_{CO_2\text{-}4A}$ activated for 5 min under CO_2 as a function of the activation temperature. Fig. 7 shows their B.E.T. surface areas and total burn-off of saccharose. The burn-off tends to increase with the activating temperature. This burn-off dependence resembles the ence of the temperature on yields of carbons produced from different lignocellulosic materials [37, 38, 55–57, 59]. The saccharose burn-off increases from a moderate value of 72% at 700°C ($A_{CO_2\text{-}4D}$) to a high value of 94% at 750°C ($A_{CO_2\text{-}4C}$) up to a maximum of 100% at 800°C ($A_{CO_2\text{-}4D}$). This trend is in line with the mechanism suggested above using reactions (7) to (11). The most important reactions are Equations 10 and 11, particularly the last, which begins to be important when the activation temperature approaches 800°C. The higher the activation temperature the more saccharose pyrolysis. In line with this behaviour, the B.E.T. surface area should decrease with increasing final activating temperature. Fig. 7, shows that these values decreases from 981 $m^2 \cdot g^{-1}$ at 700°C ($A_{CO_2\text{-}4D}$) to 717 $m^2 \cdot g^{-1}$ at 750°C ($A_{CO_2\text{-}4C}$) to zero near 800°C ($A_{CO_2\text{-}4B}$) when the macro-network pyrolyzes completely. This drastic textural change shown in B.E.T. surface area results from the destruction of the micropore texture created during the initial stages of activation by the strong oxidation conditions. The presence of potassium as KOH (that produces H_2O via reaction (7)) and the high temperatures (via reaction (11) which promotes the production of CO_2) both increase this destruction. Both oxidizing agents and activators (H_2O and CO_2) can pyrolyze the carbonaceous matrix via the two gasification reactions (8) and (10).

3.3.4. Influence of the KOH concentration

Finally, we discuss the influence of the KOH concentration on the textural changes of the macro-networks ($A_{NW\text{-}2}$) activated under N_2 at 800°C for 1 h. Fig. 8 shows the B.E.T. surface areas obtained from the adsorption isotherm of N_2 at 77°K and the total burn-off of saccharose estimated after substracting the theoretical

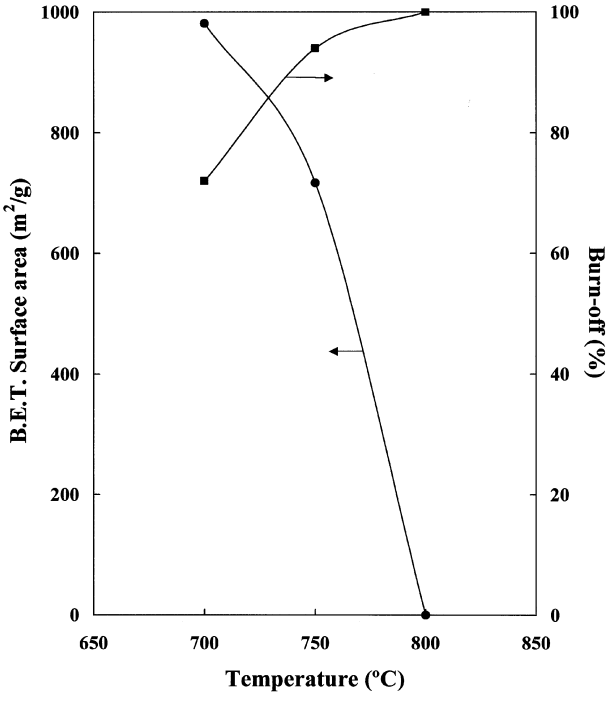

Figure 7 Surface B.E.T. areas and burn-off behaviour of networks activated with CO_2 (by 5 min) as a function of temperature.

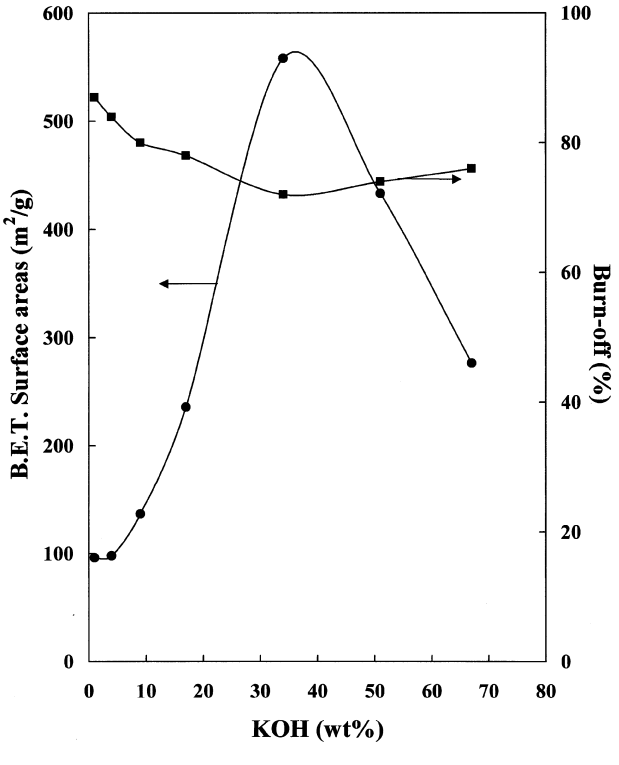

Figure 8 Surface B.E.T. areas and burn-off behaviour of networks activated with N_2 (at 800°C, by 1 h) as a function of KOH concentration.

remnant weight of potassium as K_2O, as described above. Fig. 8 shows that the burn-off decreases monotonically from a maximum of 87% at 1 wt% of KOH to a minimum of 72% at 34 wt% of KOH and then slightly increases to 76% at 67 wt% of KOH. This burn-off behaviour is very similar to that reported by Do and Ahmadpour [54] for the preparation of activated carbon from Macadamia nutshells by chemical activation with $ZnCl_2$. Fig. 8 also shows that the B.E.T. surface areas for the activated macro-networks have a volcano shaped dependence on the KOH concentration. This profile shows a low B.E.T. surface area of 96 $m^2 \cdot g^{-1}$ for 1 wt% of KOH, in line with the water washed macro-networks $A_{N_2\text{-}3}$ under the same experimental activation conditions (N_2, 800°C, 1 h) with a B.E.T. surface area of around 79 $m^2 \cdot g^{-1}$ (Table V). This result suggests that at least, some potassium as KOH is required to catalyse macro-network activation. For KOH concentrations higher that 1 wt%, the B.E.T. surface areas of the activated macro-network increase exponentially up to a maximum value of 558 $m^2 \cdot g^{-1}$ at 34 wt%. Coincidentally, this point corresponds to the concentration of KOH which has the minimum saccharose burn-off. For KOH concentrations higher than 34 wt%, the B.E.T. surface area decreases drastically to a moderate value of 276 $m^2 \cdot g^{-1}$ at 67 wt% of KOH.

These results are in line with the mechanism proposed above via reactions (7) to (9). The presence even of very low concentrations of potassium as KOH inhibits the pyrolysis of the macro-network, independently of the concentration of the hydroxide. In terms of the B.E.T. surface areas, the texture changes in the activated macro-networks in which the microporosity at low KOH concentrations increases to a maximum with increasing KOH then decreases for higher concentrations of KOH, results from the stronger oxidation conditions, favoured by very high concentrations of potassium as KOH. As reaction (7) indicates, KOH thermally decomposes to produce $K_2O + H_2O$, and gaseous water is a very efficient activator that via reaction (8) gasifies the macro-network. Another explanation of the loss of B.E.T. surface area in Fig. 8 is the well-known capacity of the alkali metals, in particular potassium, to intercalate between the parallel planes of graphite-type carbons [61–63]. Given the initial macroscopic morphology of the non-activated networks (Fig. 5), high concentrations of KOH may favour the intercalation of potassium into the macro-network sheets during activation, concominantly blocking micropores and so decreasing the surface areas as in Fig. 8. In addition, potassium-intercalation in graphite influences its hydrogen adsorption capacity [63] in line with the results in Section 3.2, that the temperature programmed reduction profile of the present macro-network of carbon shows a large negative peak at very high temperatures that is due to hydrogen evolution [28].

4. Summary and conclusion

In summary, controlled pyrolysis of saccharose produces polygonal macro-network films adhering to the bottom and walls of pyrex flasks. Our data, analysis and correlations indicate that the topological properties of these random 2D networks, composed principally of carbon aggregated grains (carbon polygrains), differ significantly from other two-dimensional cellular structures. The pentagon was the most abundant polygon in the films, with ring areas in the range of 4 to 10 mm^2 and 4 to 12 mm^2, for networks originating from saccharose pre-dissolved in water or in aqueous solution of 34 wt% KOH, respectively.

Irregular 3D sponge balls with random network structures similar to those in the films also formed at the bottom of the beakers for both samples. These sponges are assemblies of carbonaceous grains of different sizes with an interface where the carbon grains develop into a continuous 3D net of macrotubes with coiled shapes, due to the presence of potassium microparticles in the original carbonaceous matrix. The properties of these sponges indicate that they might be useful for hydrogen storage.

The activation process we present can produce activated carbons with B.E.T. surface areas as high as 850 and 981 $m^2 \cdot g^{-1}$ for activation with N_2 and CO_2, respectively, corresponding to surface areas 85 and 98 times higher than those of non-activated macro-networks. We propose that KOH catalyzes the activation of macro-networks.

Future work, identifying the effects of sample preparation, molecular weight and chemical composition of the saccharide precursors on the random cell structures of these materials will enhance our understanding of the physics of carbon networks, and probably such studies may permit us to find some connection between the topological and texture properties.

Since activated carbon materials can induce photocatalysis [64–68], and since our carbon films are transparent, we are testing the influence of our carbonaceous macro-networks on titania-photocatalyzed reactions.

Acknowledgements

Authors acknowledge to Referee of Journal of Material Science, and financial support by FONACIT.

References

1. T. HUANG, M. R. KAMAL and A. D. REY, *J. Mater. Sci. Lett.* **14** (1995) 220.
2. M. R. KAMAL, T. HUANG and A. D. REY, *J. Mater. Sci.* **32** (1997) 4085.
3. V. E. FRADKOV, M. E. GLICKSMAN, M. PALMER, J. NORDBERG and K. RAJAN, *Physica D.* **66** (1993) 50.
4. V. E. FRADKOV, A. S. KRAVCHENKO and L. S. SHVINDLERMAN, *Scripta Metall.* **19** (1985) 1291.
5. D. WEAIRE and N. RIVIER, *Contemp. Phys.* **25** (1984) 59.
6. J. STAVANS, *Rep. Prog. Phys.* **56** (1993) 733.
7. J. STAVANS and J. A. GLAZIER, *Phys. Rev. Lett.* **62** (1989) 1318.
8. D. A. NOEVER, *Phys. Review A.* **44** (1991) 968.
9. K. J. STINE, S. A. R. AUSEO, B. G. MOORE, J. A. WISE and C. M. KNOBLER, *ibid.* **41** (1990) 6884.
10. D. WEAIRE, F. BOLTON, P. MOLHO and J. A. GLAZIER, *J. Phys. Condensed Matter.* **3** (1991) 21012.
11. H. W. KROTO, J. R. HEATH, S. C. O'BRIAN, R. F. CURL and R. E. SMALLY, *Nature* **318** (1985) 162.
12. I. MOCHIDA, M. EGASHIRA, Y. KORAI and K. YOKOGAWA, *Carbon* **35** (1997) 1707.
13. E. V. OSIPOV and V. A. REZNIKOV, *ibid.* **40** (2002) 955.

14. P. J. DE PABLO, C. GÓMEZ-NAVARRO, A. GIL, J. COLCHERO, M. T. MARTINEZ, A. M. BENITO, W. K. MASER, J. GÓMEZ-HERRERO and A. M. BARÓ, *Appl. Phys. Lett.* **79** (2001) 2979.
15. Y. ZHANG, A. CHANG, J. CAO, Q. WANG, W. KIM, Y. LI, N. MORRIS, E. YENILMEZ, J. KONG and H. DAI, *ibid.* **79** (2001) 3155.
16. A. CAO, X. ZHANG, C. XU, J. LIANG, D. WU and B. WEI, *Appl. Surf. Sci.* **181** (2001) 234.
17. M. R. DIEHL, S. N. YALIRAKI, R. A. BECKMAN, M. BARAHONA and J. R. HEATH, *Angew. Chem. Int. Ed.* **41** (2002) 353.
18. R. C. BANSAL, J.-B. BONNET and F. STOECKLI, "Active Carbon" (Marcell Dekker, New York and Bansel, 1988) p. 1.
19. F. STOECKLI, *Carbon* **28** (1990) 1.
20. J. LAINE and S. YUNES, *ibid.* **30** (1990) 601.
21. J. LAINE, S. SIMONI and R. CALLES, *Chem. Eng. Commun.* **99** (1991) 15.
22. L. V. GOVOR, M. GOLDBACH, I. A. BASHMAKOV, I. B. BUTYLINA and J. PARISI, *Phys. Rev.* B **62** (2000) 2201.
23. L. J. DUNNE, P. F. NOLAN, J. MUNN, M. TERRONES, T. JONES, P. KATHIRGAMANATHAN, J. FERNANDEZ and A. D. HUDSON, *J. Phys. Condens. Matter* **9** (1997) 10661.
24. H. T. NG, M. L. FOO, A. FANG, J. LI, G. XU, S. JAENICKE, L. CHAN and S. F. Y. LI, *Langmuir* **18** (2002) 1.
25. R. IMAMURA, K. M. J. OZAKI and A. OYA, *Carbon* **37** (1999) 997.
26. L. PAN, T. HAYASHIDA and Y. J. NAKAYAMA, *Mater. Res.* **17** (2002) 145.
27. J. N. ROUZAUD and A. OBERLIN, *Carbon* **27** (1989) 517.
28. J. MATOS and J. LAINE, *J. Mater. Sci. Lett.* **17** (1998) 649.
29. J. SCHWAN, S. ULRICH, T. THEEL, H. ROTH, H. EHRHARDT, P. BECKER and S. R. P. SILVA, *J. Appl. Phys.* **82** (1997) 6024.
30. M. F. MIRI and N. RIVIER, *Europhys. Lett.* **54** (2001) 112.
31. M. A. PESHKIN, K. J. STRANDBURG and N. RIVIER, *Phys. Rev. Lett.* **67** (1991) 1803.
32. B. DUBERTRET, T. ASTE and M. A. PESHKIN, *J. Phys.* A **31** (1998) 879.
33. B. DUBERTRET, T. ASTE, H. M. OHLENBUSCH and N. RIVIER, *Phys. Rev. E* **58** (1998) 6368.
34. J. A. GLAZIER, M. P. ANDERSON and G. S. GREST, *Phil. Mag. B* **62** (1990) 615.
35. N. RIVIER, *ibid.* **52** (1985) 795.
36. J. MATOS, "Effect of Activated Carbon in Heterogeneous Photocatalytic Reactions," Ph. D. thesis, Venezuelan Institute of Scientific Research, I.V.I.C., 1999.
37. M. JAGTOYEN and F. DERBYSHIRE, *Carbon* **31** (1993) 1185.
38. J. LAINE, A. CALAFAT and M. LABADY, *ibid.* **27** (1989) 191.
39. J. LAINE, M. LABADY, F. SEVERINO and S. YUNES, *J. Catal.* **166** (1997) 384.
40. J. MATOS, J. L. BRITO and J. LAINE, *Appl. Catal. A: Gen.* **152** (1997) 27.
41. T. HUANG, T. TSUJI, M. R. KAMAL and A. D. REY, *J. Mater. Sci.* **34** (1999) 4551.
42. Z. ZHANG, B. WEI and P. M. AJAYAN, *Chem. Commun.* **9** (2002) 962.
43. S. AMELINCKX, X. B. ZHANG, D. BERNAERTS, X. F. ZHANG, V. IVANOV and J. B. NAGY, *Science* **265** (1994) 635.
44. D. BERNAERTS, X. B. ZHANG, X. F. ZHANG, S. AMELINCKX, G. VAN TENDELOO, J. VAN LANDUYT, V. IVANOV and J. B. NAGY, *Philos. Mag.* A **71** (1995) 605.
45. G. G. TIBBETTS, G. P. MEISNER and C. H. OLK, *Carbon* **39** (2001) 2291.
46. J. KUHN, *Int. J. Heat Mass Transfer* **35** (1992) 1795.
47. J. KLETT, R. HARDY, E. ROMINE, C. WALLS and T. BURCHELL, *Carbon* **38** (2000) 953.
48. A. BURIAN, P. DANIEL, S. DUBER and J. DORE, *Phil. Mag.* B **81** (2001) 525.
49. A. ALBORNOZ, M. LABADY, M. LÓPEZ, J. MATOS, F. RUETTE and J. LAINE, in "36th IUPAC Congress, Frontiers in Chemistry and New Perspectives for the 2000's" (Geneve, Switzerland, 17–22 August, 1997).
50. J. LAINE and A. CALAFAT, *Carbon* **29** (1991) 949.
51. T. WIGMANS, *ibid.* **27** (1989) 13.
52. S. J. YUHN and E. E. WOLF, *Fuel* **63** (1984) 1604.
53. F. RODRIGUEZ-REINOSO, M. MOLINA-SABIO and M. T. GONZÁLEZ, *Carbon* **33** (1995) 15.
54. A. ADMADPOUR and D. D. DO, *ibid.* **35** (1997) 1723.
55. H. TENG and H.-C. LIN, *AIChE Journal* **44** (1998) 1170.
56. A. C. LUA and J. GUO, *Carbon* **38** (2000) 1089.
57. C.-F. CHANG, C.-Y. CHANG and W.-T. TSAI, *J. Coll. Interf. Sci.* **232** (2000) 45.
58. C. MORENO-CASTILLA, F. CARRASCO-MARÍN, M. V. LÓPEZ-RAMÓN and M. A. ALVAREZ-MERINO, *Carbon* **39** (2001) 1415.
59. D. LOZANO-CASTELLÓ, M. A. LILLO-RÓDENAS, D. CAZORLA-AMORÓS and A. LINARES-SOLANO, *ibid.* **39** (2001) 741.
60. A. ROBAU SÁNCHEZ, A. AGUILAR ELGUEZABAL and L. DE LA TORRE SAENZ, *ibid.* **39** (2001) 1367.
61. L. BERNASCONI and P. A. MADDEN, *J. Phys. Chem.* B **106** (2002) 1161.
62. N. NARITA, S. NAGAI and S. SUZUKI, *Phys. Rev.* B **64** (2001) 5408.
63. H. CHENG, G. PEZ, G. KERN, G. KRESSE and J. HAFNER, *J. Phys. Chem.* B **105** (2001) 736.
64. T. TORIMOTO, S. ITOH and S. KUWABATA, *Env. Sci. Technol.* **38** (1996) 1275.
65. J. MATOS, J. LAINE and J.-M. HERRMANN, *Appl. Catal. B: Env.* **18** (1998) 281.
66. *Idem.*, *Carbon* **37** (1999) 1870.
67. J.-M. HERRMANN, J. MATOS, J. DISDIER, C. GUILLARD, J. LAINE, S. MALATO and J. BLANCO, *Catal. Today* **54** (1999) 255.
68. J. MATOS, J. LAINE and J.-M. HERRMANN, *J. Catal.* **200** (2001) 10.

Received 13 March 2003
and accepted 10 February 2004